Optimal Design in Wind Engineering Using Cyber-Physical Systems and Non-Stochastic Search Algorithms

Michael L. Whiteman, M.S., S.M.ASCE,[1] Pedro L. Fernández Cabán, Ph.D.,[2] Brian M. Phillips, Ph.D., A.M.ASCE,[3] Forrest J. Masters, Ph.D., P.E., M.ASCE,[4] Jennifer A. Bridge, Ph.D.,[5] and Justin R. Davis, Ph.D.[6]

[1]Department of Civil and Environmental Engineering, University of Maryland, 1173 Glenn L. Martin Hall, 4298 Campus Drive, College Park, MD 20742; e-mail; mlwii@umd.edu
[2]Department of Civil and Environmental Engineering, University of Maryland, 1173 Glenn L. Martin Hall, 4298 Campus Drive, College Park, MD 20742; e-mail; plferndz@umd.edu
[3]Department of Civil and Environmental Engineering, University of Maryland, 1173 Glenn L. Martin Hall, 4298 Campus Drive, College Park, MD 20742; e-mail; bphilli@umd.edu
[4]Department of Civil and Coastal Engineering, University of Florida, 365 Weil Hall, Gainesville, FL 32611-6580; e-mail; masters@eng.ufl.edu
[5]Department of Civil and Coastal Engineering, University of Florida, 365 Weil Hall, Gainesville, FL 32611-6580; e-mail; jennifer.bridge@essie.ufl.edu
[6]Department of Civil and Coastal Engineering, University of Florida, 365 Weil Hall, Gainesville, FL 32611-6580; e-mail; justin.r.davis@essie.ufl.edu

ABSTRACT

This paper explores a cyber-physical systems (CPS) approach to optimize the design of rigid, low-rise structures subjected to wind loading. The approach combines the accuracy of physical wind tunnel testing with the ability to efficiently explore a solution space using numerical optimization algorithms. The approach is fully automated, with experiments executed in a boundary layer wind tunnel (BLWT), sensor feedback monitored by a computer, and actuators used to generate physical changes to a mechatronic structural model. The approach was demonstrated for a low-rise structure with a parapet wall of variable height. A non-stochastic optimization algorithm was implemented to search along the domain of parapet heights to minimize both positive and negative pressures on the roof a of a 1:18 length scale low-rise building model. Experiments were conducted at the University of Florida Experimental Facility (UFEF) of the National Science Foundation's (NSF) Natural Hazard Engineering Research Infrastructure (NHERI) program.

INTRODUCTION

Boundary layer wind tunnels (BLWT) are the primary tool in wind engineering to characterize surface pressures on bluff bodies. BLWT modeling is valuable when studying new structures for which the simplified provisions of ASCE 7 are inadequate or too conservative (ASCE 2010). While BLWT modeling has remained a standard for decades, it has not benefited from recent advances in computationally-based optimization techniques for structural design. These techniques are now efficient enough to be applied during live testing if the structure has the ability to morph, e.g., change aerodynamic shape. Optimization algorithms have promise for

delivering cost-effective design solutions in wind engineering. The accuracy of the numerical optimization process can be improved by combining it with an experimental method such as BLWT modeling.

The objective of the study is to explore the use of cyber-physical systems (CPS) for optimal design in wind engineering. We demonstrate proof-of-concept for cyberinfrastructure-augmented BLWT modeling that produces optimal designs faster than purely experimental methods and with a higher degree of realism than purely computational methods. The approach is fully automated, with experiments executed in a BLWT, sensor feedback monitored and analyzed by a coordinating computer, and optimization techniques used to bring about physical changes to the structural model in the BLWT. Because the model is undergoing physical change as it approaches the optimal solution, this approach is given the name "loop-in-the-model" testing.

The building selected for the proof-of-concept was a low-rise structure with a parapet wall of variable height. The windward roof edges on low-rise structures cause a separation of the boundary layer and generate vortex flow with large suction loading that is particularly severe for oblique approaching wind angles. Changing the parapet height has a significant effect on these wind suction loads because it alters the location of the roof corner vortex, which mitigates extreme corner and edge suction loads with the tradeoff of increasing the downward roof loads in certain cases (Kopp et al. 2005 and Mans et al. 2005). Suction loads are damaging to components and cladding while positive pressures are additive to gravity loads. In this study, the model parapet height was adjusted automatically using servo-motors to create a particular design that is a "candidate" in the optimization framework. The building envelope was instrumented with pressure taps to measure surface pressures. The taps were densely spaced on the roof to provide sufficient resolution to capture the change in roof corner vortex formation. A golden section search (GSS) algorithm was implemented to achieve the optimum parapet height for two objective functions in two separate studies: minimizing suction on the roof and parapet surfaces, and minimizing both suction and positive pressures on the roof and parapet surfaces. Experiments were conducted in the BLWT located at the University of Florida Experimental Facility (UFEF) of the National Science Foundation's (NSF) Natural Hazard Engineering Research Infrastructure (NHERI) program.

GOLDEN SECTION SEARCH

The "loop-in-the-model" approach to optimization can be built around any optimization algorithm; the evaluation of candidate designs is replaced by experimentation on mechatronic models. Based on preliminary tests, the optimal parapet height for minimizing roof pressures is anticipated to be unimodal. GSS is a non-stochastic, deterministic optimization technique for finding the extremum of a unimodal function by successively narrowing the search space inside which the extremum is known to exist. The GSS algorithm is similar to the bisection method in that it iteratively reduces the search space, and derives its name from the fact that the length of the search space is linearly reduced each iteration by the golden ratio (Luenberger and Ye 1984). The GSS is used herein for its simplicity and to illustrate proof-of-concept. Additional studies using less restrictive metaheuristic search algorithms will be explored in the future.

In GSS, we assume that a function f is unimodal on the interval $[a, b]$. The search space is divided into three sections $[a, x_1]$, $[x_1, x_2]$, and $[x_2, b]$ by adding two intermediate points, x_1 and x_2 as shown in Figure 1. The function is then evaluated at the two intermediate points. By

evaluating the function at the two intermediate points and comparing $f(x_1)$ and $f(x_2)$, the subinterval of either $[a, x_1]$ or $[x_2, b]$ can be discarded, and the minimum (for minimization) is bracketed within the remaining subinterval (Nazareth and Tseng 2002). The locations of x_1 and x_2 are chosen so that two conditions are satisfied: x_1 and x_2 are equidistant from a and b respectively, and the ratio of lengths of the three intervals, $L/L_2 = L_2/L_1$, is constant. Based on these two conditions, $L_2 = \varphi \cong 0.618$, and $L_1 = 1 - \varphi \cong 0.382$. As a result, only one new function evaluation is needed every successive iteration as one of the previous intermediate points is reused. The two intermediate points are calculated according to the following,

$$x_1 = a + (b - a)(1 - \varphi) \tag{1}$$
$$x_2 = a + (b - a)\varphi \tag{2}$$

BLWT testing is subject to experimental error; results will vary from experiment to experiment, even for the same specimen configuration. Data may be associated with a specimen configuration that is not truly representative of that configuration. To avoid sensitivity to one non-representative test, the GSS is modified such that the previous intermediate point (which is reused) will be retested rather than directly adopted from the previous iteration.

The search space iteratively reduces around the extremum until a pre-defined tolerance for the reduction in search space is met. The tolerance is defined as the precision at the final iteration in regards to the true extremum.
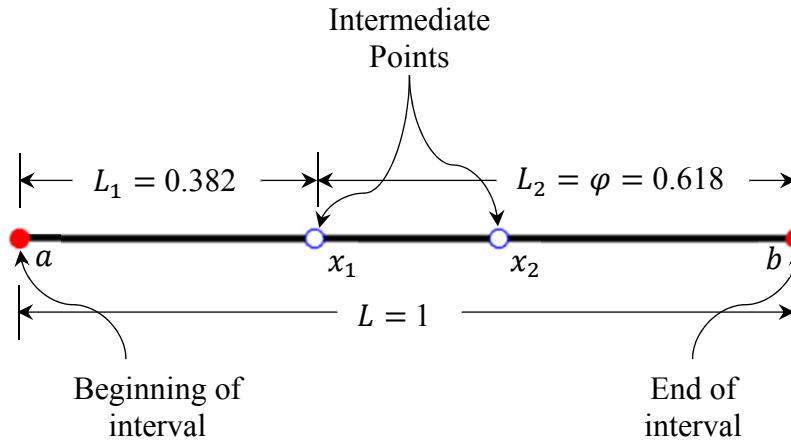

Figure 1. Sections of golden section search (GSS) for a unit interval.

PHYSICAL MODEL DEVELOPMENT

The physical model used in this study is a low-rise structure with a parapet wall of variable height. A single controllable design variable is sufficient to demonstrate proof-of-concept. By limiting the study to a single design variable, unnecessary mechanical complexity is avoided and focus is instead placed on the optimization framework.

Model actuation. The design parameter selected is the parapet wall height of a low-rise building. Candidate design solutions must be physically created in the BLWT such that their envelope wind loads are accurately measured. The outer wall of the model was actuated by four

stepper motors, one at each corner of the model. The inner core of the model remained stationary, maintaining a constant building height. As the outer wall rose above the inner model, a parapet wall was created. Strips made from polytetrafluoroethylene (PTFE) were used between the inner model and outer wall to assist in achieving smooth linear actuation. A foam gasket was used between the outer wall and the turntable to allow the outer wall to move while preventing air from leaking around the model. The model is shown in Figure 2, including the inner model (stationary) and outer wall (vertically movable).
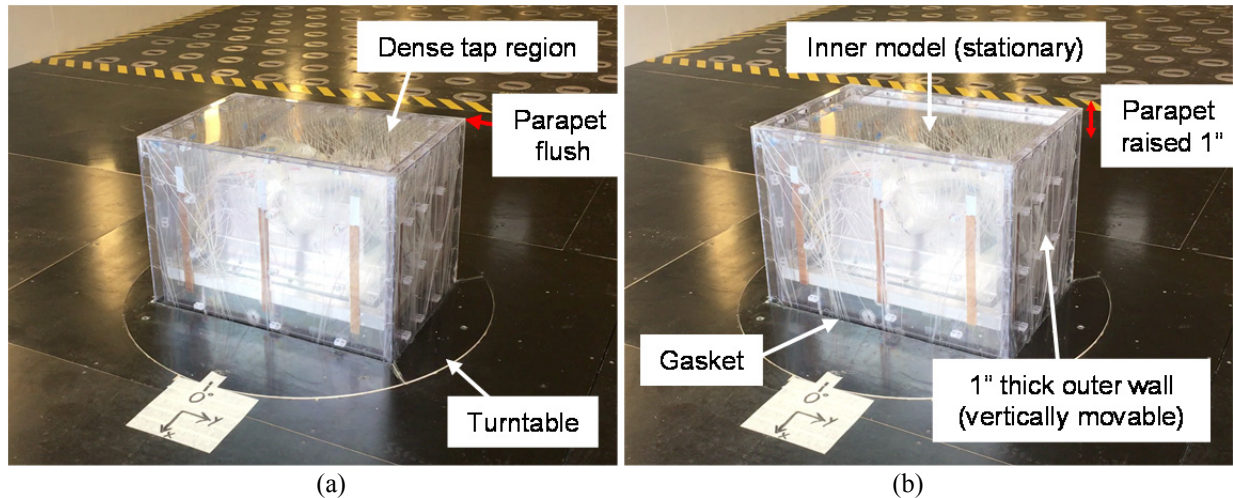

(a)   (b)

Figure 2. (a) Building model with a 0 inch parapet wall and (b) a 1 inch parapet wall – courtesy of Brian Phillips.

Nanotec stepper motors with a captured lead screw raised and lowered the outer wall around the inner core of the model to change the eave height. The motors connected to the outer wall using polycarbonate triangular supports installed in the bottom corners. A PVC pipe installed around the drive shaft of the stepper motor protected the shaft from coming into contact with any urethane pressure tap tubing during actuation. The stepper motor and its installation are shown in Figure 3.

(a)   (b)

Figure 3. (a) Stepper motor – courtesy of Nanotec (Nanotec 2017) and (b) stepper motor installed in corner of parapet wall with PVC shield – courtesy of Michael Whiteman.

4

The setup for controlling the stepper motors is given in Figure 4. Data (i.e., commands from the coordinating computer on the UF network) and power passed through a slip ring on the BLWT turntable. A Raspberry Pi 3 was mounted within the turntable to take commands from the coordinating computer and send to each of the four stepper motor controllers, which in turn actuated the stepper motors. Encoders on the stepper motors provided feedback to ensure the desired displacement was reached.
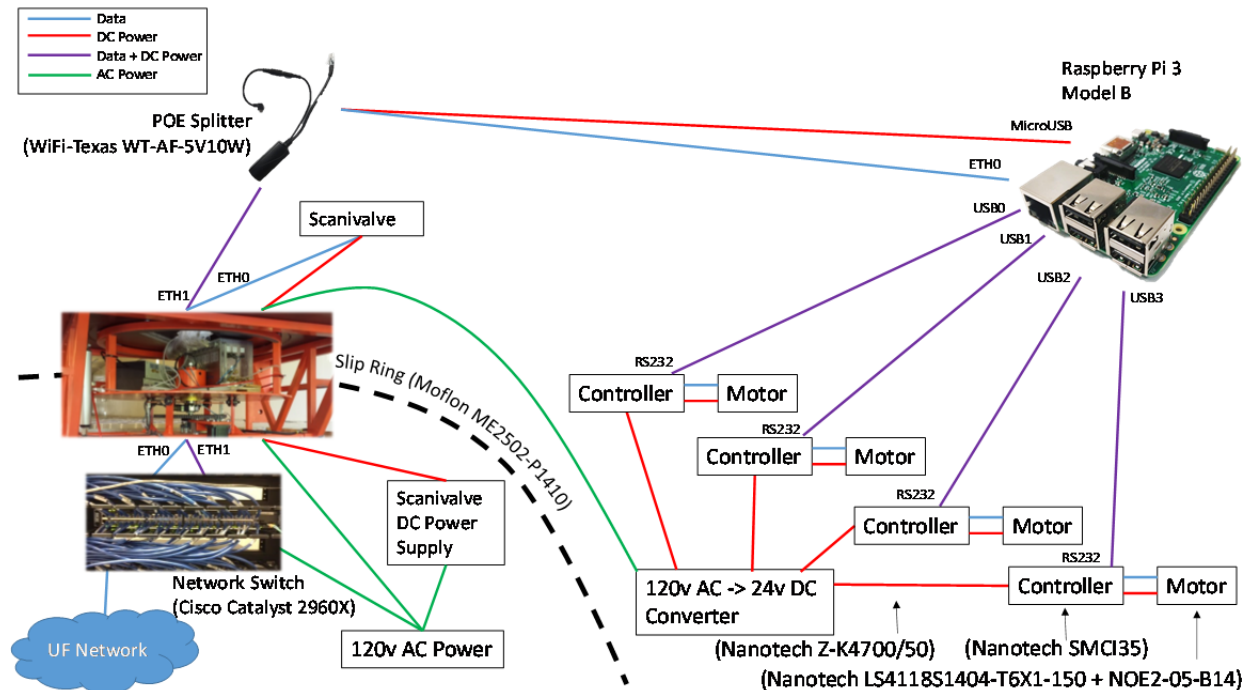

Figure 4. Wiring diagram for stepper motor control – courtesy of Michael Whiteman (upper right image), Justin Davis (upper left image), Timothy Talley (lower left image), and Pedro Fernández Cabán (middle left image).

Model Geometry. The low-rise building was modeled after a two-story office building. A length-to-width ratio of 1.5 was selected to create a rectangular building shape. Model dimensions were selected as 29.25 inches × 19.50 inches in plan with a height of 20 inches. By actuating the outer wall, a parapet wall of up to 4.5 inches model-scale was created. Urethane tubing and pressure taps were installed on the outer and inner sides of the parapet wall. A total thickness of the model parapet wall (and thus outer wall) of at least 1 inch was required to accommodate the thickness of polycarbonate sheets, metal tubulation, and minimum bend radius for the urethane tubing. The pressure taps on the outer and inner parapet walls were staggered to permit a thinner model parapet wall.

Based on the model dimensions and target design of a two-story office building, a 1:18 model-scale was selected. This corresponds to a building with full-scale dimensions of 29.6 feet × 44.4 feet in plan, 30 feet tall, and a 1.5 foot thick parapet. According to the Building Code Requirements for Masonry Structures, parapet walls should have a thickness of at least 8 inches (MSJC 2011). The building model represents a realistic two-story full-scale building with a two by three bay steel frame.

EXPERIMENTAL SETUP

Experimental Equipment. Experiments were conducted in the BLWT located at the UFEF of the NSF's NHERI program. The BLWT is 6.1 m wide with a 1 m turntable centered along the 6.1 m width 31.75 m downwind of 8 fans. The fans were kept at 1050 RPM for all testing, which corresponds to a reference height velocity of approximately 14 m/s. The pressures on the model building surfaces were measured using Scanivalve ZOC33 (Scanivalve 2016). The model building installed in the BLWT is shown in Figure 5 (a). The surface numbering of the model is given in Figure 5 (b). The walls of the building are given by Surfaces 1 to 4. As the walls extend above the roof (from actuation), Surfaces 1 to 4 also form the outer parapet walls. The inner parapet walls are given by Surfaces 6 to 9. The edges that join the outer walls (Surfaces 1 to 4) and the inner parapet walls (Surfaces 6 to 9) in Figure 5 (b) are at the same height in the model. I.e., the walls are flattened by rotating about the top of the parapet wall. Surfaces 5 and 10 are the top of the parapet wall and the roof, respectively.

(a)   (b)
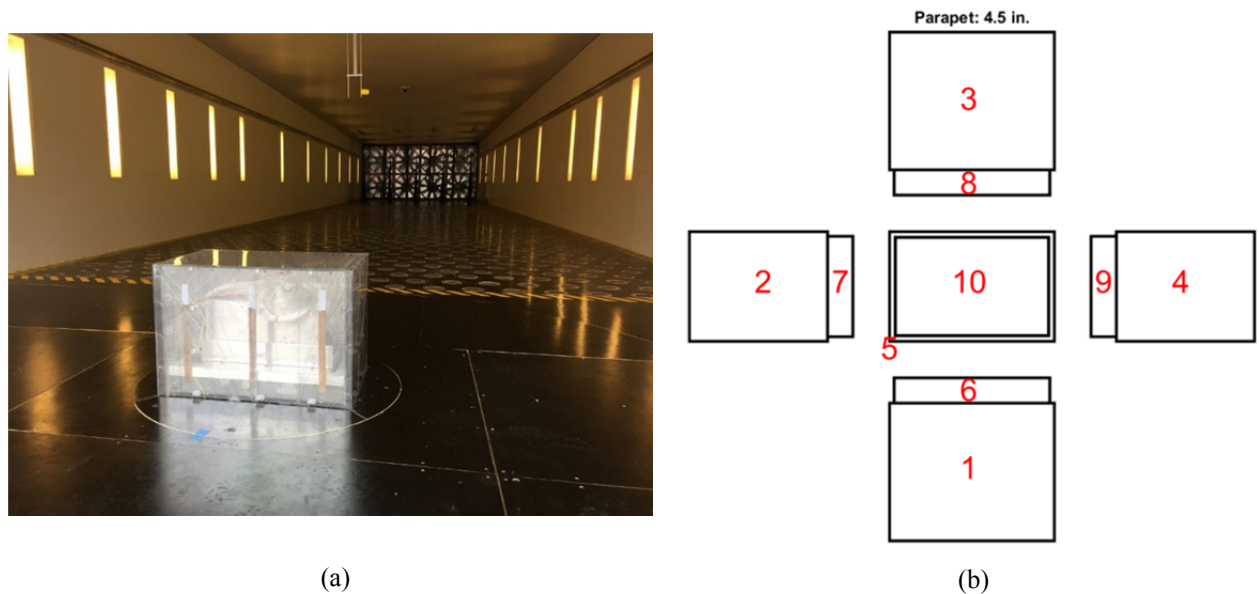
Figure 5. (a) Boundary layer wind tunnel with model low-rise building, upwind view – courtesy of Brian Phillips and (b) Surface numbering on a flattened representation of the model with a parapet of 4.5 inches – courtesy of Michael Whiteman.

Wind Simulation. Simulation of upwind terrain roughness was performed via the Terraformer, an automated roughness element grid that rapidly reconfigures the height and orientation of 1116 roughness elements in a 62×18 grid to achieve desired upwind terrain conditions (Fernández-Cabán and Masters 2017). Prior to placing the model in the tunnel, flow measurements were taken at the center of the test section using an automated gantry system instrumented with four Turbulent Flow Instrumentation Cobra pressure probes that measure u, v, and w velocity components and static pressure. For this study, roughness elements were raised to 20 mm and oriented with the wide edge perpendicular to the flow to simulate open terrain for a 1:18 length scale. Figure 6 includes the mean velocity profile and the measured longitudinal turbulence spectra at a height of 610 mm. The measured spectra was compared with the power spectra model in ESDU (ESDU 1974), and first derived by von Kármán for isotropic turbulence (Von Karman 1948). The mean velocity profile was normalized by the reference mean wind velocity U_{ref} measured at a height $z_{ref} = 1.48$ m. A roughness length estimate of 1.59 mm was obtained

6

from a non-linear least-squares fit of the log law in the inertial-sublayer (ISL) region ($z \sim 150$-900 mm), following the curve-fitting method in Karimpour et al. (2012). This results in an equivalent full-scale roughness length of 0.029 m, which is within the range of open terrain as defined in ASCE 7-10.
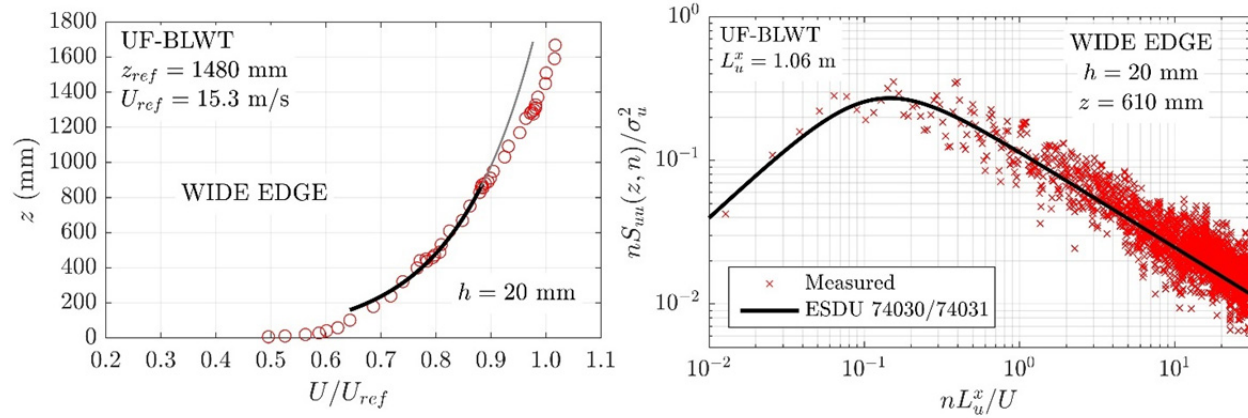

Figure 6. Mean velocity profile and longitudinal turbulence spectra (z = 610 mm) measured at the center of the test section for h = 20 mm and a wide edge windward element orientation.

Pressure Coefficients. Differential pressures from 512 taps were measured simultaneously and sampled at 625 Hz. Data was collected for 120 seconds, corresponding to approximately 660 seconds full-scale assuming a basic wind speed of 40 m/s at reference height. Pressure coefficients were referenced to the velocity pressure at the model eave height. This velocity pressure was obtained indirectly by applying a reduction factor to pitot tube measurements at the freestream (z = 1.48 m). Maximum and minimum pressure coefficients were estimated from each tap pressure time history using a Fisher-Tippett Type I (Gumbel) distribution (Cook and Mayne 1980). The C_p time history was truncated into 50 segments of equal length. The peak maximum and minimum pressure coefficients from each segment were then taken, and the 78th percentile is then used to estimate the peak maximum ($C_{p,max}$) and minimum ($C_{p,min}$) values.

OPTIMIZATION SETUP

The design domain was physically constrained to be within the model-scale parapet heights of 0 and 4.5 inches. Preliminary testing showed that as the parapet height increased, the peak suction decreased for the roof surface and top of the parapet wall and increased for the inner parapet wall surfaces. Also, peak positive pressures increased on the roof and inner parapet walls with increasing parapet height. Critical $C_{p,min}$ and $C_{p,max}$ values were observed for the roof, inner parapet wall, and top of parapet at approach wind angles of 45° and 90°. Thus, to minimize the number of BLWT runs, each candidate solution was only evaluated at 45° and 90°.

The objective function was selected as a minimization of the maximum magnitude of peak pressures on the roof, inner parapet walls, and top of the parapet considering the wind angles of 45° and 90° for two cases: suction only (Case 1), and both suction and positive pressure (Case 2). For both cases the search space was initially defined as [0, 4.50] to ensure that the solution was physically feasible. A convergence tolerance of 0.001 inches was selected based on the rated precision of 0.01 inches for the Nanotec stepper motors. Based upon the desired tolerance and

7

linear reduction of the search space, a total of 18 design iterations were determined to be necessary.

OPTIMIZATION RESULTS

Minimize Peak Suction (Case 1). Large suction can be damaging to components and cladding or contribute to windborne debris. Increasing the parapet height will reduce the suction on the roof surface, a major benefit of installing parapet walls. At the same time, increasing the parapet height will increase the suction on the inner parapet walls. This balance creates the design tradeoff explored in Case 1. The objective is selected as a minimization of the maximum magnitude of the peak suction considering the roof, inner parapet walls, and the top of the parapet. The convergence of the search space towards the optimum height of 2.80 inches is shown in Figure 7. As previously mentioned, the initial domain bounds (iteration 1) were [0, 4.50]. At iteration 1, the intermediate points produced parapet heights of $h_p = 1.72$ inches and 2.78 inches based upon calculations according to Eq. (1) and (2). The measured $C_{p,min}$ of the two intermediate points were 4.71 and 4.24 (Table 1). Since the objective function was to reduce $C_{p,min}$ (suction only for Case 1), $h_p = 2.78$ inches was the better candidate design than 1.72 inches. As a result, the domain [0, 1.72] was discarded and the bounds for the next iteration (iteration 2) became [1.72, 4.50]. This procedure was repeated for the maximum number of iterations.

Peak suction values for both intermediate points at each iteration are shown in Table 1. The variability of peak suction due to the experimental testing is seen for iterations 12 through 18, as both intermediate points have the same parapet heights for these iterations. Despite being at the same height, the measured $C_{p,min}$ for iterations 12 through 18 vary between intermediate points and across iterations. Figures 8 and 9 depict the envelope plot of the $C_{p,min}$ for the optimal parapet height at 45° and 90° respectively. This illustrates the balance in large magnitudes of $C_{p,min}$ on the roof and top of the parapet wall (Figure 8) and inner parapet wall surfaces (Figure 9). Lowering the parapet would increase suction on the roof at 45° while raising the parapet would increase suction on the inner parapet wall at 90°. This balance is expected because the suction on the roof, top of the parapet, and inner parapet walls were given equal weight in the objective function. The optimal result corresponds to a full-scale parapet height of 4.20 feet. This parapet height simultaneously minimizes suction on the roof and inner parapet walls. According to the Building Code Requirements for Masonry Structures, the height of structural parapets should not exceed 3 times their thickness (MSJC 2011). The optimal height found satisfies this limit of 4.5 feet as applied to the current building.
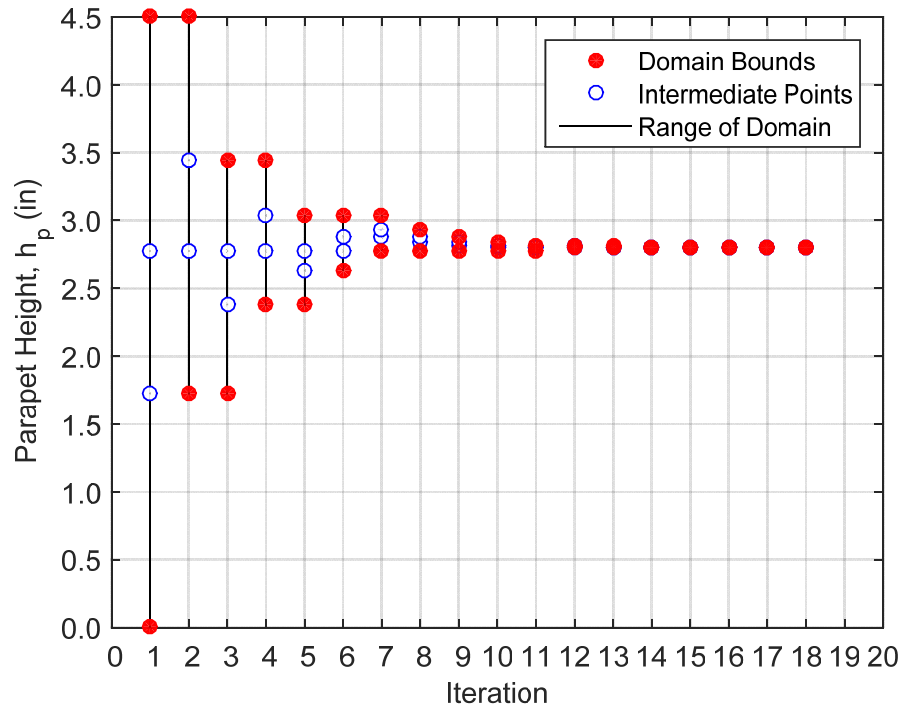
Figure 7. Parapet height iteration history using GSS (Case 1).

Table 1. Parapet height and $C_{p,min}$ for each iteration using GSS (Case 1).

Iteration	Intermediate Point, x_1		Intermediate Point, x_2	
	h_p [in]	$C_{p,min}$	h_p [in]	$C_{p,min}$
1	1.72	4.71	2.78	4.24
2	2.78	4.48	3.44	4.67
3	2.38	4.36	2.78	3.94
4	2.78	3.94	3.03	4.23
5	2.63	4.16	2.78	4.12
6	2.78	4.16	2.88	4.03
7	2.88	4.34	2.94	4.35
8	2.84	4.18	2.88	4.35
9	2.82	3.82	2.84	3.91
10	2.80	3.84	2.82	3.89
11	2.80	4.18	2.80	3.91
12	2.80	3.97	2.80	4.05
13	2.80	4.09	2.80	4.42
14	2.80	4.04	2.80	4.03
15	2.80	3.84	2.80	4.23
16	2.80	3.93	2.80	3.81
17	2.80	3.90	2.80	3.96
18	2.80	4.10	2.80	4.38

Parapet: 2.80 in., Wind angle: 45°, Min Cp
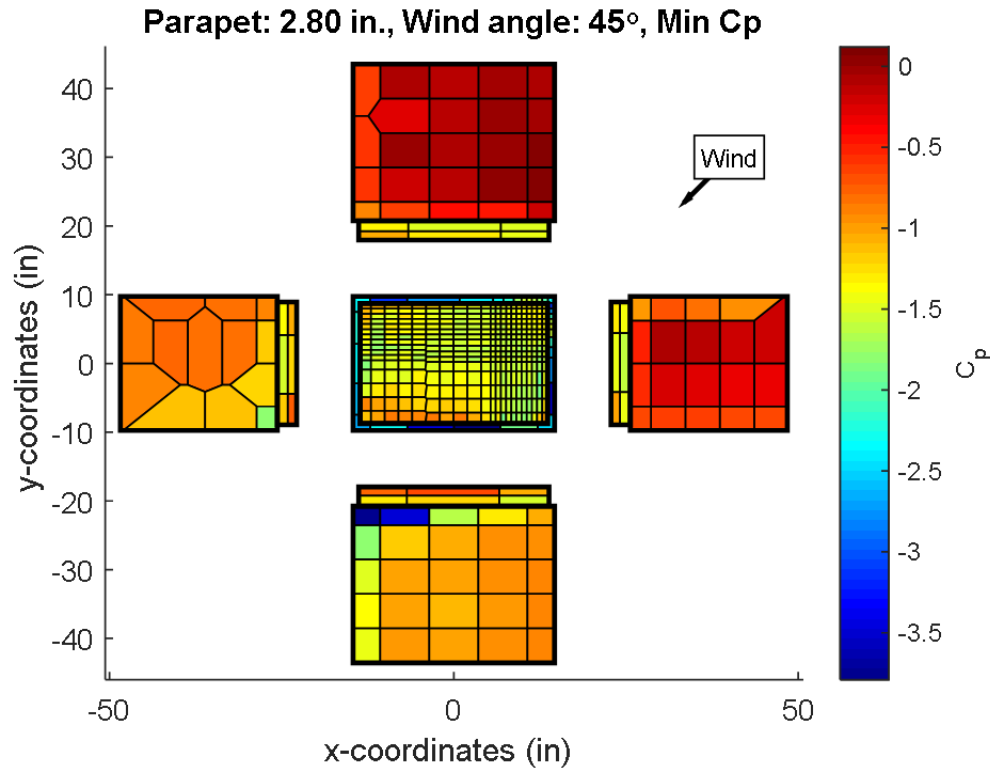
Figure 8. $C_{p,min}$ **for optimal parapet height, 45° wind angle shown.**

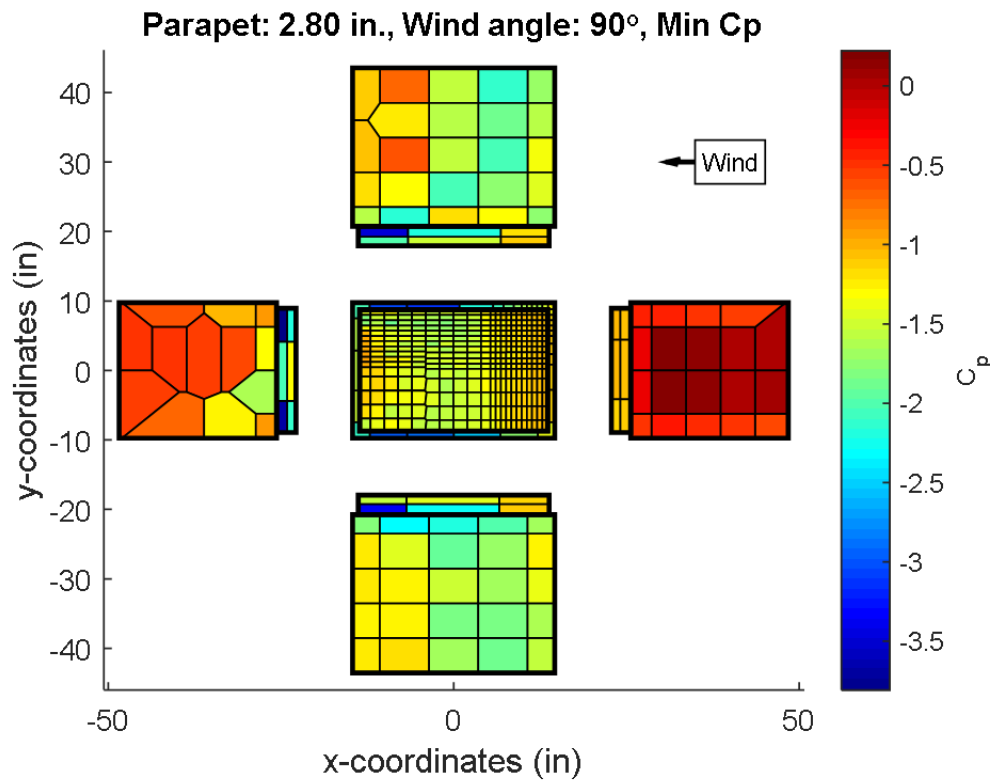**Parapet: 2.80 in., Wind angle: 90°, Min Cp**

Figure 9. $C_{p,min}$ **for optimal parapet height, 90° wind angle shown.**

Minimize Suction and Positive Pressure (Case 2). This case includes the design tradeoffs regarding peak suction from Case 1. In addition, Case 2 considers positive pressure. As the parapet height increases, the positive pressure increases for the roof and the windward side of the leeward parapet. Positive pressures on the roof are additive to gravity loads, which can increase the forces on structural members. Positive pressures on the windward side of the leeward parapet wall are additive to the base moment of the parapet wall. Formally, the objective of Case 2 is to minimize the maximum magnitude of peak suction and peak positive pressures on the roof, inner parapet walls, and top of the parapet. The relative importance of reducing suction versus positive pressure is not considered; they are treated equally.

The convergence of the search space towards the optimum height of 2.71 inches is shown in Figure 10. The maximum of ($|C_{p,min}|$, $|C_{p,max}|$) for both intermediate points at each iteration is shown in Table 2. Similar to Case 1, there is variability of the maximum suction due to the experimental testing best seen for iterations 12 through 18. For both angles of 45° and 90° the peak suction on the surfaces considered is greater in magnitude than the peak positive pressure and therefore governs the design. The results for the envelope of peak suction pressures at the optimal parapet height are similar to those of Figures 8 and 9. The optimal height corresponds to a full-scale parapet height of 4.05 feet, which satisfies the limit of 4.5 feet according to the Building Code Requirements for Masonry Structures as applied to the current building (MSJC 2011).
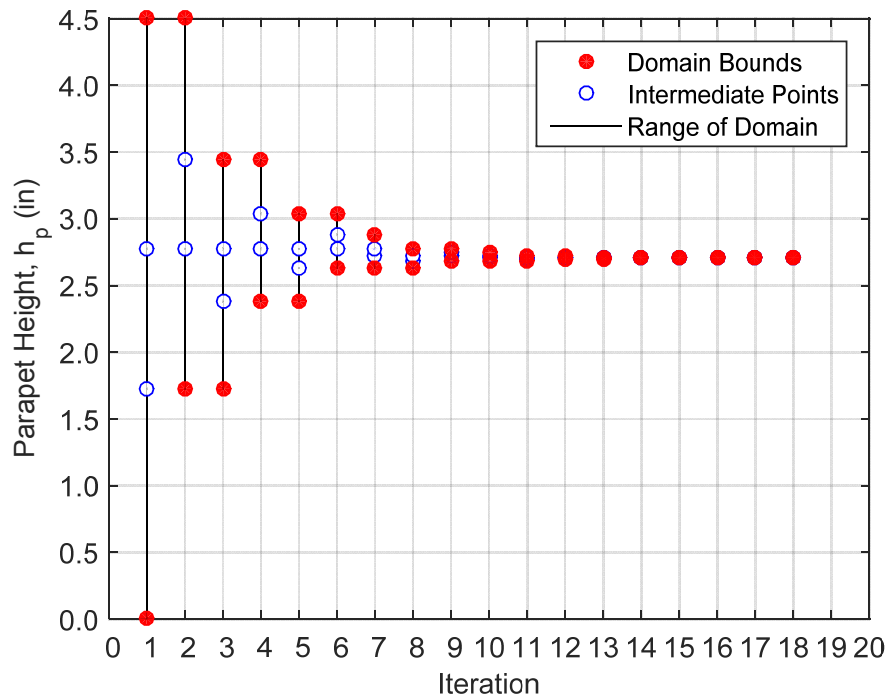

Figure 10. Parapet height iteration history using GSS (Case 2).

11

Table 2. Parapet height and max($|C_{p,min}|$, $|C_{p,max}|$) for each iteration using GSS (Case 2).

Iteration	Intermediate Point, x_1		Intermediate Point, x_2	
	h_p [in]	max($|C_{p,min}|$, $|C_{p,max}|$)	h_p [in]	max($|C_{p,min}|$, $|C_{p,max}|$)
1	1.72	4.69	2.78	3.94
2	2.78	4.28	3.44	4.88
3	2.38	4.57	2.78	3.93
4	2.78	4.16	3.03	4.35
5	2.63	4.21	2.78	4.19
6	2.78	4.25	2.88	4.36
7	2.72	4.00	2.78	4.20
8	2.69	3.95	2.72	3.95
9	2.72	4.11	2.74	4.24
10	2.71	4.00	2.72	4.02
11	2.71	3.99	2.71	3.96
12	2.71	3.82	2.71	3.89
13	2.71	4.11	2.71	4.03
14	2.71	3.99	2.71	4.02
15	2.71	4.02	2.71	4.20
16	2.71	4.06	2.71	4.16
17	2.71	4.00	2.71	3.98
18	2.71	3.96	2.71	4.03

CONCLUSIONS

This study investigates the application of a non-stochastic search algorithm to the cyber-physical optimization of buildings subject to wind loading. The building selected for proof-of-concept is a low-rise building with adjustable parapet height. The approach combines the accuracy of physical wind tunnel testing with the ability to efficiently explore a solution space using numerical optimization algorithms. The creation and evaluation of candidate designs is completed physically in a BLWT using a 1:18 length scale mechatronic building model. The analysis of data, calculation of objective functions, and determination of new candidate designs is completed numerically. A non-stochastic GSS algorithm was applied to minimize peak roof and parapet wall pressures. The GSS-based approach was demonstrated to automatically guide the physical structure to an optimal state based on user-defined objectives and constraints. Based on the objective functions and constraints chosen, optimal parapet heights of 2.80 inches model-scale and 4.20 feet full-scale (Case 1) and 2.71 inches model-scale and 4.07 feet full-scale (Case 2) were found for the low-rise structure studied using the GSS algorithms. The findings are potentially significant for more complex structures where the optimal solution may not be obvious and cannot be easily determined with traditional experimental or computational methods.

ACKNOWLEDGEMENTS

REFERENCES

American Society of Civil Engineers. (2014). *Minimum design loads for buildings and other structures,* Standard ASCE/SEI 7-10. Third printing. ASCE, Reston, VA.

Cook, N. J., & Mayne, J. R. (1980). A refined working approach to the assessment of wind loads for equivalent static design. *Journal of Wind Engineering and Industrial Aerodynamics*, *6*(1-2), 125-137.

ESDU. Characteristics of atmospheric turbulence near the ground. Part I: definitions and general information, *Engineering Sciences Data Unit*, Itm. No. 74030, 74031, 1974, London, UK.

Fernández-Cabán, P. L., & Masters, F. J. (2017). Near surface wind longitudinal velocity positively skews with increasing aerodynamic roughness length. *Journal of Wind Engineering and Industrial Aerodynamics*, *169*, 94-105.

Karimpour, A., Kaye, N. B., & Baratian-Ghorghi, Z. (2012). Modeling the neutrally stable atmospheric boundary layer for laboratory scale studies of the built environment. *Building and Environment, 49*, 203-211.

Kopp, G. A., Mans, C., & Surry, D. (2005). Wind effects of parapets on low buildings: Part 2. Structural loads. *Journal of wind engineering and industrial aerodynamics*, *93*(11), 843-855.

Kopp, G. A., Mans, C., & Surry, D. (2005). Wind effects of parapets on low buildings: Part 4. Mitigation of corner loads with alternative geometries. *Journal of Wind Engineering and Industrial Aerodynamics*, *93*(11), 873-888.

Kopp, G. A., Surry, D., & Mans, C. (2005). Wind effects of parapets on low buildings: Part 1. Basic aerodynamics and local loads. *Journal of Wind Engineering and Industrial Aerodynamics*, *93*(11), 817-841.

Luenberger, D. G., & Ye, Y. (1984). *Linear and nonlinear programming* (Vol. 2). Reading, MA: Addison-wesley.

Mans, C., Kopp, G. A., & Surry, D. (2005). Wind effects of parapets on low buildings: Part 3. Parapet loads. *Journal of wind engineering and industrial aerodynamics*, *93*(11), 857-872.

Nanotec. (2017). LS41: Linear Positioning Drive: NEMA 17. Retrieved from http://us.nanotec.com/products/710-ls41-linear-positioning-drive-nema-17/

Nazareth, L., & Tseng, P. (2002). Gilding the lily: A variant of the Nelder-Mead algorithm based on golden-section search. *Computational Optimization and Applications*, *22*(1), 133-144.

Masonry Standards Joint Committee (MSJC). (2011). Building code requirements for masonry structures (TMS 402-11/ACI 530-11/ASCE 5-11). *The Masonry Society, Boulder, CO.*

Scanivalve. (2016). ZOC3 miniature pressure scanner. Retrieved from http://scanivalve.com/products/pressure-measurement/miniature-analog-pressure-scanners/zoc33-miniature-pressure-scanner/

Von Karman, T. (1948). Progress in the statistical theory of turbulence. *Proceedings of the National Academy of Sciences*, *34*(11), 530-539.